Radio recombination line observations at $1.0 - 1.5\,\mathrm{GHz}$ with FAST

Chuan-Peng Zhang[1,2], Jin-Long Xu[1,2], Guang-Xing Li[3], Li-Gang Hou[1], Nai-Ping Yu[1,2] and Peng Jiang[1,2]

[1] National Astronomical Observatories, Chinese Academy of Sciences, Beijing 100101, China; *cpzhang@nao.cas.cn*
[2] CAS Key Laboratory of FAST, National Astronomical Observatories, Chinese Academy of Sciences, Beijing 100101, China
[3] South-Western Institute for Astronomy Research, Yunnan University, Kunming 650500, China

Abstract H II regions made of gas ionized by radiations from young massive stars, are widely distributed in the Milky Way. They are tracers for star formation, and their distributions are correlated with the Galactic spiral structure. Radio recombination lines (RRLs) of hydrogen and other atoms allow for the most precise determination of physical parameters such as temperature and density. However, RRLs at around 1.4 GHz from H II regions are weak and their detections are difficult. As a result, only a limited number of detections have been obtained yet. The 19-beam receiver on board of the Five-hundred-meter Aperture Spherical radio Telescope (FAST) can simultaneously cover 23 RRLs for H$n\alpha$, He$n\alpha$, and C$n\alpha$ ($n = 164 - 186$), respectively. This, combined with its unparalleled collecting area, makes FAST the most powerful telescope to detect weak RRLs. In this pilot survey, we use FAST to observe nine H II regions at L band. We allocate 20 minutes pointing time for each source to achieve a sensitivity of around 9 mK in a velocity resolution of $2.0\,\mathrm{km\,s^{-1}}$. In total, 21 RRLs for H$n\alpha$ and C$n\alpha$ at $1.0 - 1.5\,\mathrm{GHz}$ have been simultaneously detected with strong emission signals. Overall, the detection rates for the H167α and C167α RRLs are 100%, while that for the He167α RRL is 33.3%. Using hydrogen and helium RRLs, we measure the electron density, electron temperature, and pressure for three H II regions. This pilot survey demonstrates the capability of FAST in RRL measurements, and a statistically meaningful sample with RRL detection, through which knowledge about Galactic spiral structure and evolution can be obtained, is expected in the future.

Key words: telescopes: FAST — H II regions — radio lines: ISM — galaxies: star formation

1 INTRODUCTION

Galactic H II regions are made of gas ionized young massive stars. They are tracers for star formation, their evolutions are interesting from an astrophysical point of view, and their distributions are correlated with the Galactic spiral structure (e.g., Churchwell et al. 2006, 2007; Beaumont & Williams 2010; Hou & Han 2014; Zhang et al. 2014, 2017). H II regions are ubiquitously distributed in the Milky Way. The Wide-Field Infrared Survey Explorer (WISE) catalog of H II regions (Anderson et al. 2014) is the largest sample of Galactic H II region candidates to date. The sample is distributed throughout the Milk Way disk, making them ideal tracers for the Galactic spiral structure. Determining their distances and physical parameters is thus crucial.

Radio recombination lines (RRLs) of hydrogen provide the simplest and most precise method of determining the electron temperature and density of H II regions. Unlike observations of optical emission lines, RRLs are unaffected by reddening from interstellar dust. Further, they can be accurately measured even in weak astronomical sources (Gordon & Sorochenko 2002), allowing for accurate determination of the physical parameters. RRLs are distributed in a wide range of frequencies. Recent RRL surveys at different wavelengths were performed with highly sensitive facilities to study H II regions (e.g., Anderson et al. 2011, 2014; Liu et al. 2013; Alves et al. 2015; Chen et al. 2020). However, the RRLs at around 1.4 GHz from H II regions are relatively weak (Anderson et al. 2011), thus either large telescopes or long integration are needed to detect them. Before FAST, these observations are difficult, and only a small sample of H II regions is detected at ~1.4 GHz.

The Five-hundred-meter Aperture Spherical radio Telescope (FAST) is located at geographic latitude of $25°39'10''6$ and its observable maximum zenith angle is $40°$ (Nan et al. 2011; Jiang et al. 2019, 2020), thus FAST observation can cover all the H II regions distributed in the Galactic longitude range of around $21°$ to $223°$.

Table 1 Sources and Observational Results

Source	R.A.(J2000)	Dec.(J2000)	Velocity	T_A (H167α)	FWHM	T_A (C167α)	FWHM	T_A (He167α)	FWHM
	hh:mm:ss	dd:mm:ss	km s^{-1}	K	km s^{-1}	K	km s^{-1}	K	km s^{-1}
G43.148+0.013	19:10:10.98	+09:05:18.2	10.47	0.244	28.26	0.074	18.07		
G43.177−0.008	19:10:18.73	+09:06:13.4	15.07	0.242	29.04	0.066	16.64		
G48.905−0.261	19:22:07.85	+14:03:12.6	60.78	0.203	27.71	0.028	34.13		
G48.946−0.331	19:22:27.89	+14:03:24.9	65.85	0.251	26.53	0.045	14.18	0.017	6.02
G48.991−0.299	19:22:26.22	+14:06:42.2	66.61	0.229	28.80	0.038	13.07	0.020	5.55
G49.028−0.217	19:22:12.74	+14:10:58.4	61.91	0.295	21.26	0.047	11.93	0.017	5.07
G49.224−0.334	19:23:01.08	+14:18:00.6	63.43	0.154	30.58	0.037	31.37		
G49.368−0.303	19:23:11.17	+14:26:32.6	49.47	0.226	29.71	0.049	29.15		
G49.466−0.408	19:23:45.74	+14:28:45.2	56.66	0.169	25.84	0.053	23.23		

Notes: Only the $n = 167$ data for H$n\alpha$, He$n\alpha$, and C$n\alpha$ RRLs are listed above, because other transitions have a very close spectral information to the $n = 167$.
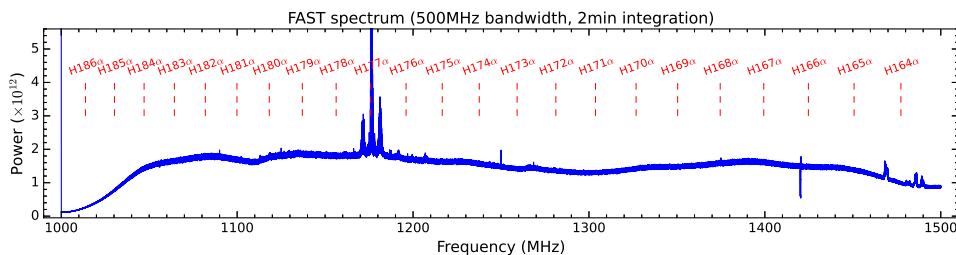

Fig. 1 H$n\alpha$ ($n = 164 − 186$) RRLs in a FAST spectrum for G43.148+0.013. The *blue spectrum* shows original and uncalibrated data with 500 MHz bandwidth and two minutes integration from FAST observations.

The 19-beam receiver of the FAST has a band width of 500 MHz with a frequency range of $1.0 − 1.5$ GHz (Jiang et al. 2019, 2020), which can simultaneously cover 23 RRLs for H$n\alpha$, C$n\alpha$, and He$n\alpha$ (principal quantum number $n = 164 − 186$), respectively. This makes FAST the most powerful telescope to detect weak RRLs at L band. Therefore, a larger population of H II regions deserves to be systematically studied with FAST. Using the RRLs and continuum emission at around 1.4 GHz, we could measure the pressure, evolutionary ages, distances, and relative abundance of elements in H II regions. With a reasonably-sized sample, we could determine the distribution of them in the Milky Way disk and correlate it with the physical parameters of the H II regions. This will deepen our understanding of the co-evolution between H II regions and the Milky Way.

In this work, as a pilot study, nine H II region candidates are selected from a $4 − 6$ GHz RRL survey with Shanghai Tianma 65 m telescope by Chen et al. (2020), where RRLs such as H$n\alpha$, He$n\alpha$, and C$n\alpha$ ($n = 98 − 113$) have been detected (see Table 1). We observe $1.0 − 1.5$ GHz (see Table 2) RRLs using FAST to determine the physical parameters and to provide the first constraint on the expected detection rate.

2 OBSERVATIONS AND DATA REDUCTION

2.1 Observations with FAST

The FAST observations were conducted between 2020 Aug.28 and Sep.19. We used tracking mode to point to each target using the central beam (Beam-M01) of the 19-beam receiver on FAST. Other beams were used as off-source observations to calibrate the data in Beam-M01. This setup could save lots of observation time. The half-power beamwidth (HPBW) is ∼2.9′ at 1.4 GHz, and the pointing error is ∼0.15′ (Jiang et al. 2019, 2020). For the backend, a high spectral resolution (1048576 channels), full bandwidth (500 MHz), and dual polarization mode were used to collect the observational signal, resulting a frequency resolution of 476 Hz or a velocity resolution of ∼0.1 km s^{-1} at 1.4 GHz. Each source was integrated for 20 minutes with a sampling rate of one second. For intensity calibration, noise signal with amplitude of 1 K was injected under a period of two seconds in only first two minutes at the beginning of each source observation. The relevant degrees per flux unit factor (DPFU) for Beam-M01 is DPFU ∼ 16.02 ± 0.26 Kelvin per Jy beam^{-1} at 1400 MHz (Jiang et al. 2020).

2.2 Data Reduction

Our selected sources have extremely strong continuum emission ($\gtrsim$10 Jy), this leads to that the total fluxes with noise diode at switch-on and switch-off states have no obvious discrepancy. Thus, our observational data could not be calibrated directly by noise diode. This issue could be solved by using the simultaneously observed data in other beams to calibrate our target data from the central beam, assuming that all data from each beam have the same rms. We could firstly calibrate data from the FAST

Table 2 The Rest Frequencies for H$n\alpha$, He$n\alpha$, and C$n\alpha$ RRLs

Transition n	$\nu_{Hn\alpha}$ (MHz)	$\nu_{Hen\alpha}$ (MHz)	$\nu_{Cn\alpha}$ (MHz)
164	1477.335	1477.937	1478.072
165	1450.716	1451.307	1451.440
166	1424.734	1425.314	1425.444
167	1399.368	1399.938	1400.066
168	1374.600	1375.161	1375.286
169	1350.414	1350.964	1351.088
170	1326.792	1327.333	1327.454
171	1303.718	1304.249	1304.368
172	1281.175	1281.697	1281.815
173	1259.150	1259.663	1259.778
174	1237.626	1238.130	1238.243
175	1216.590	1217.086	1217.197
176	1196.028	1196.515	1196.625
177	1175.927	1176.406	1176.514
178	1156.274	1156.745	1156.851
179	1137.056	1137.520	1137.624
180	1118.262	1118.718	1118.820
181	1099.880	1100.328	1100.429
182	1081.898	1082.339	1082.438
183	1064.307	1064.740	1064.838
184	1047.094	1047.521	1047.617
185	1030.251	1030.671	1030.765
186	1013.767	1014.180	1014.273

Reference: Müller et al. (2005)

Beam-M16 receiver (Jiang et al. 2020) to get the antenna temperature (T_A) using:

$$T_A = T_{noise} \times \frac{\text{Power}_{cal\,off}}{\text{Power}_{cal\,on} - \text{Power}_{cal\,off}}, \qquad (1)$$

where T_{noise} is the injected noise temperature of known, Power$_{cal\,on}$ and Power$_{cal\,off}$ are, respectively, the observed total power for noise diode with switch-on and switch-off. Assuming that the FAST Beam-M01 data have the same rms as the Beam-M16, we then could calibrate the observed data in the Beam-M01 using the Beam-M16[1]. Such calibration method may introduce an uncertainty of 30% into the derived antenna temperature. Finally, we smoothed the spectral data into a resolution (channel width) of 10 KHz, corresponding to a spectral resolution of around 2.0 km s^{-1} at 1.4 GHz. The sensitivity achieves to around 9 mK at such conditions.

3 ANALYSIS AND DISCUSSION

3.1 RRLs in FAST Spectral Observations

Figure 1 presents one FAST spectrum including the whole 500 MHz bandwidth and using two minutes integration toward H II region G43.148+0.013. H$n\alpha$ ($n = 164 - 186$) RRLs are indicated in the spectrum. Additional bonus is the carbon and helium RRLs, which could be simultaneously covered together with the hydrogen RRLs. This means that the FAST observation could simultaneously cover 23 hydrogen, carbon and helium

---

[1] For a test, we also use other beam data to calibrate the Beam-M01 data, there is no obvious discrepancy in the final results.

RRLs, respectively. However, some frequencies are often polluted by the radio frequency interference (RFI). For example, at around 1175 MHz, H177α RRL is always seriously polluted by communication satellites. This will lead to that one often cannot see the seriously polluted emission lines, for example, H177α RRL.

3.2 Hydrogen, Carbon and Helium RRLs

Figure 2 presents the detected RRLs toward the H II region G43.148+0.013. The positions of H$n\alpha$, He$n\alpha$, and C$n\alpha$ RRLs with $n = 164 - 186$ (except $n = 177, 180$) have been indicated in each panel. For the RRLs with $n = 177$ and $n = 180$, they have been seriously polluted by RFI, so they are not given here. The rest frequencies of H$n\alpha$, He$n\alpha$, and C$n\alpha$ ($n = 164 - 186$) lines are listed in Table 2. Figure 3 shows the detected H167α, He167α, and C167α RRLs in nine sources (see Table 1) and their Gaussian fitting results. We can see that the He167α RRL was detected in only three sources (G48.946−0.331, G48.991−0.299, and G49.028−0.217), while H167α and C167α RRLs were detected in all the nine sources. The detection rates are respectively 33.3% for He167α RRL, and 100% for H167α and C167α RRLs in our selected nine samples.

Information obtained from hydrogen RRLs enables us to determine the basic physical conditions of H II regions as well as distribution of ionized hydrogen in Galaxy (Brown et al. 1978; Zhang et al. 2014; Oonk et al. 2017; Xu et al. 2020). Helium, the second-most abundance element of the interstellar medium (ISM), is also ionized in the majority of H II regions. The ratio of the integrated intensities of hydrogen and helium RRLs enables us to accurately determine the relative abundance of helium, which has great significance not only for understanding the physics of the ISM, but also for understanding how the Universe formed. In three sources, we simultaneously detected and then measured their line ratios (listed in Table 3), which are respectively around 0.0154, 0.0168, and 0.0137 in G48.946−0.331, G48.991−0.299, and G49.028−0.217. This means that in such H II regions there is $\langle \frac{N(He^+)}{N(H^+)} \rangle \sim 1.5\%$, which is consistent with the investigations for other giant H II regions in Galactic center (Churchwell et al. 1974).

Gordon & Sorochenko (2002) found that the centroids of the carbon line emission are offset from that of the hydrogen line emission, the radial velocities were often different from the hydrogen RRLs, and the line widths were always much narrower. Although the carbon lines were spatially associated, they probably did not come from the region of the H II gas itself. For these reasons, Zuckerman & Palmer (1968) suggested that the carbon lines originated from the outer parts of a dense HI region bounding the discrete H II regions. Comparing the centroids and line widths of the carbon and hydrogen
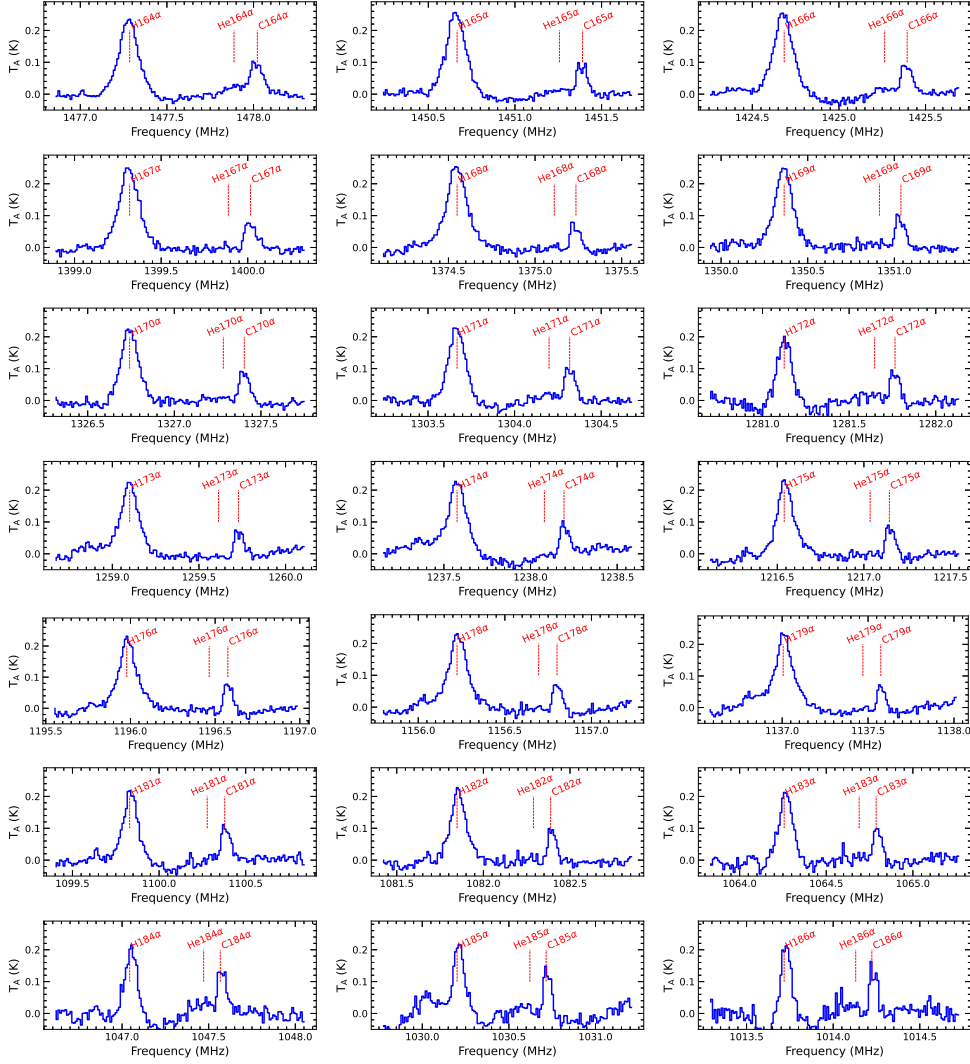
Fig. 2 Detected RRLs toward G43.148+0.013. The positions of H$n\alpha$, He$n\alpha$, and C$n\alpha$ RRLs with $n = 164 - 186$ (except $n = 177, 180$, which are polluted by RFIs.) have been indicated in each panel.

167α RRLs for all sample, we found that there exist velocity offsets within $\pm 10\,\mathrm{km\,s^{-1}}$ between them, and that the carbon line widths were indeed narrower than those for the hydrogen RRLs. This indicates that the C II and H II regions are formed in different layers of molecular clouds. For example, Alves et al. (2015) suggested the C II regions may be formed in the outer and cooler layers of molecular clouds at the boundaries with H II regions. The helium and hydrogen 167α RRLs have a close line-center velocity, indicating that they may be originated from the same region.

3.3 Electron Density, Electron Temperature, and Pressure

Interstellar bubbles (H II regions in nature) surrounding OB stars are the result of the combined effects of radiation pressure and stellar winds (Zhang et al. 2013, 2016, 2019).

The expansion of bubbles will lead to changes in the dust-to-gas ratio, due to movement of the grains from one zone to another, as well as because of grain destruction (Draine 2011). In the outer part of bubbles, Draine (2011) and Zhang & Wang (2013) detected the drift speeds become small as being away from the bubble. Radiation pressure acting on gas and dust causes H II regions to have central densities that are lower than the density near the ionized boundary (Draine 2011; Dutta et al. 2018). Since the effects of radiation pressure are not negligible, the observed cavity must be the result of the combined effects of radiation pressure and a stellar wind.

For optically thin ionized gas and local thermodynamic equilibrium (LTE) condition, one could derive the electron temperature T_e based on the ratio between 1.4 GHz continuum flux density and H167α line intensity
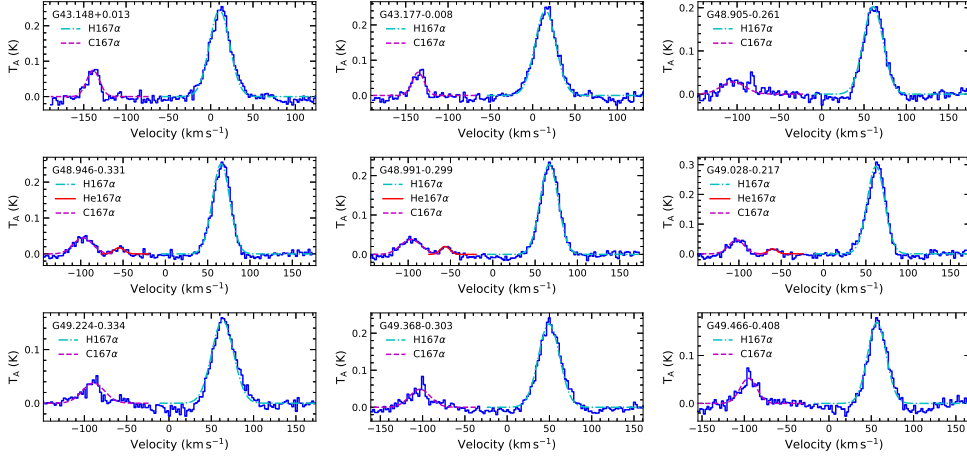
Fig. 3 Detected H167α, He167α, and C167α RRLs in nine sources and their Gaussian fitting results. The velocity at 0 km s^{-1} corresponds to 1399.368 MHz, which is the rest frequency of H167α.

Table 3 Physical Features for Three H II Regions

Source	Distance (kpc)	$\frac{N(\text{He}^+)}{N(\text{H}^+)}$	$\frac{T_{1.4\text{GHz}}}{T_{\text{H}167\alpha}}$	T_e (K)	EM (pc cm^{-6})	n_e (cm^{-3})	P_e (Pa)
G48.946−0.331	5.3 ± 0.2	0.0154	81.5	7900	5.4×10^4	153	3.3×10^{-11}
G48.991−0.299	5.3 ± 0.2	0.0168	77.9	7064	4.5×10^4	139	2.7×10^{-11}
G49.028−0.217	5.3 ± 0.2	0.0137	75.6	8986	6.1×10^4	162	4.0×10^{-11}

References for distance: Sato et al. (2010), Anderson et al. (2014), Chen et al. (2020).

(Gordon & Sorochenko 2002; Zhang et al. 2014) with

$$T_e = \left[\left(\frac{6985}{\alpha(\nu, T_e)} \right) \left(\frac{\Delta V_{\text{H}167\alpha}}{\text{km s}^{-1}} \right)^{-1} \left(\frac{T_{1.4\text{GHz}}}{T_{\text{H}167\alpha}} \right) \left(\frac{\nu}{\text{GHz}} \right)^{1.1} \right.$$
$$\left. \times \left(1 + \frac{N(\text{He}^+)}{N(\text{H}^+)} \right)^{-1} \right]^{0.87}, \tag{2}$$

where $\alpha(\nu, T_e) \sim 1$ is a slowly varying function tabulated by Mezger & Henderson (1967), $\frac{N(\text{He}^+)}{N(\text{H}^+)} \sim 0.015$ (see Sect. 3.2), $\Delta V_{\text{H}167\alpha}$ is the FWHM of H167α RRL, and the ratio $\frac{T_{1.4\text{GHz}}}{T_{\text{H}167\alpha}}$ could be directly measured from the observations, where we ignore the relatively weak background contribution into the 1.4 GHz continuum. Finally we get the electron temperature T_e listed in Table 3.

The emission measure (EM) could be derived (e.g., Wilson et al. 2009; Zhang et al. 2014) with

$$\text{EM} = 7.1 \text{ pc cm}^{-6} \left(\frac{S_L}{\text{Jy}} \right) \left(\frac{\lambda}{\text{mm}} \right) \left(\frac{T_e}{\text{K}} \right)^{1.5}$$
$$\times \left(\frac{\Delta V}{\text{km s}^{-1}} \right) \left(\frac{\theta_s}{\text{arcsec}} \right)^{-2}. \tag{3}$$

For the H167α line, the peak line intensity is S_L and the line width ΔV are listed in Table 1. The observing wavelength is $\lambda = 21$ cm. Based on the parameters above, we could obtain an EM. The intrinsic size θ_s could be derived from the radius of an H II region. Our selected H II regions have larger size than the telescope beam (3′), thus we could assume $\theta_s = 1.5'$ for estimation. The

corresponding volume electron density is estimated by n_e from

$$\text{EM} = n_e^2 L f_V, \tag{4}$$

where we could assume the path length as $L = D \times \tan(\theta_s)$ (D is the source distance listed in Table 3) and volume filling factor as $f_V = 1$.

The pressure P_e from the ionized gas can be estimated following:

$$P_e = 2 n_e k_b T_e, \tag{5}$$

where electron density n_e and electron temperature T_e have been derived and listed in Table 3. If not measured, T_e can be inferred from the Galactocentric distance of a source using R_{gal}: $T_e = 278 \text{ K} \times (R_{\text{gal}}/\text{kpc}) + 6080 \text{ K}$ (Tremblin et al. 2014). Comparing the two methods, the derived electron temperatures in our work are consistent with that. Given a larger sample, we could estimate the mid-plane pressure as a function of Galactocentric distance (Wolfire et al. 2003) and test the fitting formula in Tremblin et al. (2014). This will also help us to further understand the distribution of n_e and T_e in the Milky Way.

4 SUMMARY

The FAST telescope has a large collecting area and enables high-sensitivity observations for extended sources. The 19-beam receiver has a wide bandwidth (500 MHz) and it can simultaneously cover 23 H$n\alpha$, He$n\alpha$, and C$n\alpha$ ($n = 164 - 186$) RRLs, respectively. This combination is ideal for the

systematical study of RRLs from Galactic H II regions. In this pilot study, we observe nine H II regions using hydrogen, carbon and helium RRLs. Using 20 minutes pointing time for each source, a sensitivity of around 9 mK with a spectral resolution of around $2.0 \, \text{km s}^{-1}$ can be achieved. In total, 21 RRLs for H$n\alpha$ and C$n\alpha$ at $1.0 - 1.5 \, \text{GHz}$ have been simultaneously detected in strong emission except two lines ($n = 177$ and $n = 180$), which are seriously polluted by RFI. Overall, the detection rates for the He167α and C167α RRLs are 100%, while that for the He167α RRL is 33.3% in our selected sample.

Comparing the centroids and line widths of the carbon and hydrogen 167α RRLs for all sample, we found that there exist velocity offsets between -10 and $+10 \, \text{km s}^{-1}$. This indicates that the C II and H II regions are formed in different layers of molecular clouds. Using the hydrogen and helium RRLs, we have measured electron density, electron temperature, and pressure (listed in Table 3) in three H II regions. This pilot study proves that the survey for a large sample of statistical measurement is feasible in the future.

In a future FAST work, we plan to observe a statistically significant sample of H II regions to measure electron density, electron temperature, pressure, evolutionary stages, and the relative abundance of elements. The sample would allow us to study the distribution of these physical parameters (including line widths, line ratios, electron temperatures and densities) in various parameter spaces, as well as the relation between the physical properties of H II and their locations measured in terms of, for example, the Galactocentric distance, to understand the co-evolution between the H II regions and the Galactic disk.

References

Alves, M. I. R., Calabretta, M., Davies, R. D., et al. 2015, MNRAS, 450, 2025

Anderson, L. D., Bania, T. M., Balser, D. S., & Rood, R. T. 2011, ApJS, 194, 32

Anderson, L. D., Bania, T. M., Balser, D. S., et al. 2014, ApJS, 212, 1

Beaumont, C. N., & Williams, J. P. 2010, ApJ, 709, 791

Brown, R. L., Lockman, F. J., & Knapp, G. R. 1978, ARA&A, 16, 445

Chen, H.-Y., Chen, X., Wang, J.-Z., Shen, Z.-Q., & Yang, K. 2020, ApJS, 248, 3

Churchwell, E., Mezger, P. G., & Huchtmeier, W. 1974, A&A, 32, 283

Churchwell, E., Povich, M. S., Allen, D., et al. 2006, ApJ, 649, 759

Churchwell, E., Watson, D. F., Povich, M. S., et al. 2007, ApJ, 670, 428

Draine, B. T. 2011, ApJ, 732, 100

Dutta, S., Mondal, S., Samal, M. R., & Jose, J. 2018, ApJ, 864, 154

Gordon, M. A., & Sorochenko, R. L. 2002, Radio Recombination Lines, Their Physics and Astronomical Applications, 282

Hou, L. G., & Han, J. L. 2014, A&A, 569, A125

Jiang, P., Tang, N.-Y., Hou, L.-G., et al. 2020, RAA (Research in Astronomy and Astrophysics), 20, 064

Jiang, P., Yue, Y., Gan, H., et al. 2019, Science China Physics, Mechanics, and Astronomy, 62, 959502

Liu, B., McIntyre, T., Terzian, Y., et al. 2013, AJ, 146, 80

Mezger, P. G., & Henderson, A. P. 1967, ApJ, 147, 471

Müller, H. S., Schlöder, F., Stutzki, J., & Winnewisser, G. 2005, Journal of Molecular Structure, 742, 215

Nan, R., Li, D., Jin, C., et al. 2011, International Journal of Modern Physics D, 20, 989

Oonk, J. B. R., van Weeren, R. J., Salas, P., et al. 2017, MNRAS, 465, 1066

Sato, M., Reid, M. J., Brunthaler, A., & Menten, K. M. 2010, ApJ, 720, 1055

Tremblin, P., Anderson, L. D., Didelon, P., et al. 2014, A&A, 568, A4

Wilson, T. L., Rohlfs, K., & Hüttemeister, S. 2009, Tools of Radio Astronomy (Springer-Verlag)

Wolfire, M. G., McKee, C. F., Hollenbach, D., & Tielens, A. G. G. M. 2003, ApJ, 587, 278

Xu, J.-L., Xu, Y., Jiang, P., et al. 2020, ApJL, 893, L5

Zhang, C.-P., Li, G.-X., Wyrowski, F., et al. 2016, A&A, 585, A117

Zhang, C.-P., Li, G.-X., Zhou, C., Yuan, L., & Zhu, M. 2019, A&A, 631, A110

Zhang, C.-P., & Wang, J.-J. 2013, RAA (Research in Astronomy and Astrophysics), 13, 47

Zhang, C.-P., Wang, J.-J., & Xu, J.-L. 2013, A&A, 550, A117

Zhang, C.-P., Wang, J.-J., Xu, J.-L., Wyrowski, F., & Menten, K. M. 2014, ApJ, 784, 107

Zhang, C.-P., Yuan, J.-H., Xu, J.-L., et al. 2017, RAA (Research in Astronomy and Astrophysics), 17, 057

Zuckerman, B., & Palmer, P. 1968, ApJL, 153, L145